Feasibility assessment of pervaporation for desalinating high-salinity brines

Emily Huth, Satish Muthu, Luke Ruff and Jonathan A. Brant

ABSTRACT

Pervaporation, which is a non-pressure driven membrane process, was evaluated to determine its viability for desalinating high-salinity source waters like those originating from oil and natural gas development (produced water). Two types of membrane material chemistries were studied in order to identify the optimal properties for maximizing the permeate flux under a given set of operating conditions. Permeate flux was determined to be a significant function of membrane thickness and the diffusion coefficient of water through the membrane. The diffusion coefficient is in turn a function of the membrane's affinity for water (hydrophilicity) and its fractional free volume space. A cellulose triacetate membrane (Membrane B) achieved fluxes of 0.06 m^3 m^{-2} day^{-1} when treating solutions having salt concentrations of 100 g L^{-1}, comparable to fluxes achieved by other types of non-pressure driven membrane processes. The flux increased in a linear fashion with decreasing ionic strength and improved through increases in the vapor pressure gradient and/or inclusion of a feed channel spacer into the test cell. Salt rejection efficiencies by all membranes were >99%; however, co-ions were able to penetrate into the membrane material matrix over time.

Key words | desalination, pervaporation, produced water

Emily Huth
Satish Muthu
Luke Ruff
Jonathan A. Brant (corresponding author)
Department of Civil and Architectural Engineering,
University of Wyoming,
1000 E. University Avenue,
Laramie,
WY 82071,
USA
E-mail: jbrant1@uwyo.edu

NOMENCLATURE

D_i	Diffusion coefficient of water across a polymeric membrane
y_{io}	Activity coefficient of water in bulk solution
γ_{io}^G	Gas phase activity coefficient of water
J_i	Flux of component i across a semi-permeable membrane
K_i^G	Sorption coefficient of component i between the gas and membrane phases
m_i	Molecular weight of water
ρ_m	Molar density of the polymeric membrane material
p_{io}	Vapor pressure of water (liquid) at membrane-feed interface
p_{il}	Vapor pressure of water (vapor) at membrane-permeate interface
$p_{i\text{sat}}$	Saturation vapor pressure of water vapor
l	membrane thickness
ΔVP	Vapor pressure gradient across a membrane
ΔP	Hydraulic pressure gradient across a membrane

$\Delta \pi$	Osmotic pressure gradient across a membrane
μ	Dynamic viscosity of water
θ	Contact angle
n	Number of repeats
R_m	Hydraulic resistance of a membrane
T	Temperature
Z	Atomic number

INTRODUCTION

Rapid development of domestic oil and natural gas resources has made possible a future in which the United States is energy independent (International Energy Agency 2012). There are a number of environmental challenges that are associated with energy development such as groundwater contamination from hydraulic fracturing (Kharak *et al.* 2013), air pollution through flaring of waste

gas (McKenzie *et al.* 2012), and disposal or reuse of produced waters (Beckman *et al.* 2013). Developing economical and sustainable technologies for managing the large volumes of water that are co-generated with oil and natural gas is perhaps the most perplexing of these challenges. This is due to the high total dissolved solids (TDS) concentrations that characterize many of these waters (Benko & Drewes 2008), which makes them difficult to treat using conventional desalination processes like reverse osmosis (RO).

The TDS concentration in conventional produced waters can be in excess of 50,000 mg L^{-1} (Benko & Drewes 2008). High TDS concentrations are problematic for conventional desalting membrane processes like RO, as the hydraulic pressures required to overcome the osmotic pressure of the feed solution are prohibitively high. Overcoming the challenges presented by high TDS source waters has resulted in the development of non-pressure driven processes like membrane distillation (MD) (Singh & Sirkar 2012; Adham *et al.* 2013; Alkhudhiri *et al.* 2013), forward osmosis (FO) (Hickenbottom *et al.* 2013; McGinnis *et al.* 2013) and more recently pervaporation (PV) (Korin *et al.* 1996; Korngold *et al.* 1996; Zwijnenberg *et al.* 2005; Drobek *et al.* 2012). Evaporative processes such as MD and PV are particularly attractive for desalinating high-salinity brines as they do not have to overcome the osmotic pressure of the feed solution nor must they rely on the creation of a suitably high osmotic gradient across the membrane to achieve a reasonable flux. Additionally, non-pressure driven processes are touted as being more resistant to certain types of fouling relative to pressure driven ones (Lee *et al.* 2010).

Pervaporation involves the permeation of a solvent across a semi-permeable and nonporous membrane by solution-diffusion, followed by its evaporation into a vapor phase (Mondal *et al.* 2008). Specific components in a mixed solution are rejected by the membrane as a result of their lower affinity with and/or diffusivity through the membrane relative to another solvent as described in the solution-diffusion model for mass transport across nonporous membranes (Shao & Huang 2007). For desalination applications the membrane has a high affinity for water (i.e. hydrophilic). Thus, water permeates through the membrane by the solution-diffusion mechanism, while salts are rejected. Mass transport is driven by a vapor pressure gradient

(ΔVP) that exists between the feed and permeate streams. A low absolute pressure is maintained on the permeate side of the membrane in order to maintain a high ΔVP (Shao & Huang 2007). This is achieved using a dry and cold sweeping gas or by applying a vacuum. Pervaporation has been used in the separation of organic solutions, particularly dehydration of organic solvents, removal of dilute organic compounds from aqueous streams and organic–organic mixture separation (Lipski & Cote 1990; Slater *et al.* 2006); however, its use in desalination systems has been less extensive (Korngold *et al.* 1996; Drobek *et al.* 2012).

Korngold *et al.* (1996) examined the performance of a nonporous proton exchange membrane in a pervaporation desalination application to elucidate the roles played by membrane characteristics (thickness, charge density) and operating conditions (temperature, feed water salinity, and sweep gas velocity) on water flux. Permeate fluxes ranged from 1.33×10^{-2} to 7.88×10^{-2} m^3 m^{-2} day^{-1}. The water flux increased with increasing velocity of the sweeping gas. The flux did plateau at a sweeping gas velocity of 2 m s^{-1}, which was attributed to hydraulic resistance that was imposed by the hollow fiber membrane. In other words, the transport of the water through the membrane became dependent on the transport of the liquid within the membrane independent of the air velocity. The permeate flux also increased with decreasing membrane wall thickness and increasing water temperature, but it decreased with increasing salt concentration (0–3 M NaCl) in the feed water. Increasing water flux with decreasing wall thickness is due to a reduction in the hydraulic resistance of the membrane. The relationship between water salinity and flux is less clear. These authors determined that the flux was ultimately limited by the properties of the membrane material (fractional free volume and affinity with water).

While salt rejection efficiencies for different membranes in pervaporation desalination applications have been reported to be ≥99%, evidence does exist that, depending on the membrane properties and process operation, solutes are capable of penetrating into the membrane structure, particularly for hydrophilic materials (Quinones-Bolanos *et al.* 2005a, b; Zwijnenberg *et al.* 2005). The ability of salts to penetrate nonporous FO membranes has also been documented (McCutcheon & Elimelech 2006). There are a variety of possible avenues or mechanisms by which salts and other

dissolved substances could penetrate into hydrophilic, non-porous membrane material (Michaels *et al.* 1965; Voros *et al.* 1996; Zhang *et al.* 2007). It is possible that the salt molecules could be adsorbed into the membrane material, thereby passing through the polymer matrix by diffusion exactly the same way that water molecules are transported through the membrane. For salt passage to occur, there are a number of important factors, which serve to affect membrane properties and the way the dissolved substance interacts with it. These factors are temperature, free-volume space within the membrane, hydrated size of the dissolved substance, hydrophilicity of the membrane and substance (i.e. affinity of substance to membrane material), and possible charge interactions between the membrane and substance. In a previous study by Ju *et al.* (2010), it was observed that as the permeability of a membrane increased (due to greater amounts of free volume space in a membrane or differences in membrane structure), the ability of the membrane to selectively transport water over salts decreased (i.e. the rejection capabilities decreased). It is also possible that the salt molecules could fit within the microcavities or free-volume space within the polymer material of the membrane and then travel through the membrane material by means of diffusion.

The purpose of this work was to characterize the performance of two different types of polymeric membrane materials in pervaporation desalination applications in order to determine their feasibility for treating produced waters. Our efforts were focused on high-salinity solutions that were representative of conventional produced waters. Using established pervaporation performance models, we elucidated the fundamental properties of each material that affected the water flux in pervaporation. Performance and modeling results were then used to identify the ideal membrane properties for desalinating high-salinity source waters in an effort to guide future membrane development.

METHODS

Water uptake by membranes (swelling analysis)

The swelling analysis was one method that was used to characterize affinity of each membrane with water as a function of solution ionic strength. For the swelling tests, flat-sheet membrane samples were cut into squares having dimensions of 5×5 cm. For Membrane A, three samples of each membrane thickness ($l = 20, 50, 90$ and $250\ \mu m$) were analyzed. Membrane samples were weighed dry following storage in a desiccator cabinet for at least 24 h. Test solutions used for the swelling analysis included doubly deionized water (DDW) and sodium chloride solutions of varying ionic strengths (10, 100, and 1000 mM NaCl). Membrane samples were periodically removed from a given test solution over a total of 3 days and weighed. All tests were conducted at a temperature (T) of $23 \pm 2\ ^{\circ}C$. The amount of water associated with the support structure for Membrane B was not separately accounted for in the water uptake measurements.

Membrane surface chemistry

The affinity of each membrane for water (i.e. hydrophilic character) was determined using contact angle (θ) measurements with water. Contact angle measurements were performed using an Easy Drop Goniometer (Krüss Scientific) on flat-sheet membrane samples using the captive bubble technique (Brant & Childress 2002). All membrane samples were first soaked in DDW for a minimum of 48 h and then installed in the sample stage, which was then submerged into water. DDW (pH = 5.5, $T = 23\ ^{\circ}C$) was used as the probe liquid for all contact angle measurements. Three air bubbles (volume = $5\ \mu L$) were analyzed per membrane sample in which a minimum of five membrane samples were characterized in order to calculate an average contact angle value ($n \geq 15$). Tangential streaming potential measurements (Surpass Electrokinetic Analyzer, Anton Paar, Ashland, VA) were carried out on flat-sheet membrane samples. Prior to analysis the membrane samples were soaked for at least 24 h in the background electrolyte solution that was to be used in the streaming potential measurement. Samples were rinsed with DDW prior to loading them into the clamped sample cell. The streaming potential was then measured at two different solution ionic strengths (1 and 10 mM KCl) as a function of solution pH through automatic titration of either KOH or HCl.

Membrane surface morphology and elemental composition

The morphology and elemental composition of virgin and fouled membrane samples were determined using a field emission scanning electron microscope (FESEM, Quanta FEG MK2 Scanning Electron Microscope, FEI, Eindhoven), which incorporated an integrated energy dispersive X-ray analysis accessory (EDS, Oxford Instruments X-Max EDS Detector, Model #51-XMX0005, Concord, MA). Analyses were carried out on the membrane surfaces as well as on the cross sections of each membrane to characterize the extent to which different ions penetrated into the membrane material matrix. When performing FESEM-EDS analysis of the membrane cross sections, elemental mapping was completed for the entirety of the cross section as well as at select spots throughout the thickness of the membrane sample. Images of each sample were taken using two different detectors: an Everhart-Thronley detector (ETD) and a backscatter electron detector (BSED). ETD images show the shapes and textures of items that are in the image, while BSED images show locations in the images that have higher average atomic numbers (Z) than the average Z of the sample. Locations in the image with proportionally high Z, for example, a salt crystal on the surface of the membrane, appear brighter than the locations with lower Z values.

Test solutions

Membrane performance tests were carried out using simple electrolyte (sodium chloride, purity $= 99\%$) solutions of varying concentrations. These solutions were prepared using reagent grade sodium chloride, which was added to DDW to achieve a desired concentration. Salt concentrations were selected to represent those found in conventional produced waters, which are typically $\leq 150\ \mathrm{g\ L^{-1}}$ (Benko & Drewes 2008; Clark & Veil 2009; Yang *et al.* 2011). Tests were performed using sodium chloride concentrations that ranged from 0 to $100\ \mathrm{g\ L^{-1}}$ NaCl. All test solutions were unbuffered and thus solution pH was equal to pH 5.5 ± 0.5, unless noted otherwise.

Membranes

Two different types of membrane materials were studied: Membrane A was a nonporous membrane having a symmetric structure. Membrane A was constructed of a thermoplastic block copolymer of the polyester family (Du-Pont de Nemours International SA, Geneva). Membrane B was a cellulose triacetate membrane having an embedded polyester screen support (Hydration Technology Innovations, Scottsdale, AZ). FESEM images of the cross sections of Membranes A and B are shown in Figure 1.
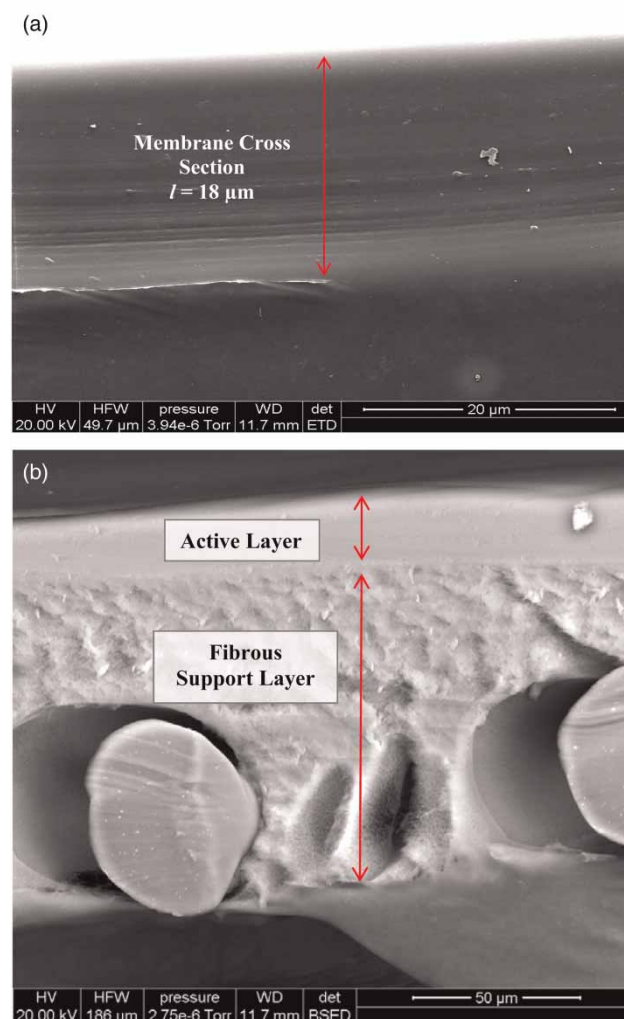

Figure 1 | FESEM images of the cross sections of (a) the 20 μm thick polyester membrane and (b) the cellulose triacetate membrane. The cellulose triacetate membrane has an active layer thickness of 10 μm with a porous/fibrous support layer having a thickness of 105 μm.

The thickness of Membrane A was varied, having values of 20, 50, 90, and 250 μm. Results referring to a specific thickness for Membrane A will be noted as such by including the thickness value as a subscript (e.g. Membrane $A_{20\,\mu m}$). Both membranes had isoelectric points (pH_{iep}) between approximately pH 2–3 and were negatively charged over the solution pH and ionic strengths evaluated here.

Dead end filtration apparatus

The specific flux of the flat-sheet pervaporation membranes was evaluated using a dead end filtration apparatus. Membrane samples were soaked in DDW for at least 24 h prior to being used in the experiments. Membrane samples were placed in the dead end filtration cell (HP4750, Sterlitech, Kent, WA) and supported using a stainless steel porous plate. Pressure was applied to the feed solution using compressed nitrogen. Flux was measured at the following pressure values: 68, 172, 345, 689, 1,034, and 1,379 kPa. The specific flux was calculated as the slope of a linear fit to the data (flux as a function of pressure) using regression analysis. Pressure and the water flux through the membrane were recorded as a function of time using a data acquisition program that was designed using LabView 2012. Flux was determined by measuring the change in permeate mass over time using a mass balance that was connected to a computer, the density of water at a given temperature ($T = 23 \pm 2\,°C$), and the known active area of the membrane sample (14.6 cm^2).

Cross flow pervaporation test unit

A schematic of the cross flow pervaporation test unit used for assessing membrane performance is given in Figure 2. Prior to each test, membrane samples were cut and hydrated by soaking them in DDW for at least 24 h. Two flat-sheet test cells (CF042A-FO, Sterlitech Corporation) were used with each having an active membrane area of 0.0084 m^2. The CF042A-FO test cells incorporated a flow channel in the feed and permeate lines and thus allowed for the sweeping gas to flow across the permeate side of the membrane. The sweeping gas flowed through the permeate channel and was used to maintain a constant vapor pressure gradient across the pervaporation membrane. Compressed air was passed through a Drierite Dryer Column (size 8 mesh, Cole-Parmer, Vernon Hills, IL) to remove any moisture prior to it entering the test cells. After the compressed air was passed through the drying column, the sweeping gas had a relative humidity of 2% resulting in a vapor pressure of water (vapor) at the membrane–permeate interface (p_{il}) = 55.5 to 60.8 Pa (Table 1). The range in reported values for p_{il} is due to variations in room temperature during the course of the tests. The sweeping gas velocity was held constant for all tests unless otherwise noted at a value of 4.68×10^{-3} m s^{-1}. The feed water flow rate to each test cell was 0.35 L min^{-1}, corresponding to a cross flow velocity of 0.056 m s^{-1}. Permeate from the test cells was collected using a liquid nitrogen cold trap, and the permeate was quantified by sealing the condensing vessel and weighing it before and after each test. The feed solution was housed in a 2-L jacketed-reactor (Ace Glass, Vineland, NJ), which included a mixer for maintaining a homogeneous composition and an external heat exchanger (recirculating heater/chiller) for temperature control. System parameters, including feed water conductivity, pressure, flow rate, and temperature were all measured using in-line probes and meters.

RESULTS AND DISCUSSION

Water uptake by membrane materials as a function of solution ionic strength

Membrane A was found to readily absorb water as illustrated by an average increase in membrane material mass of $30 \pm 2\%$ following immersion in DDW for 3 days. Following a two tailed *t*-test of the data ($n = 5$), it was determined that there was no statistical difference in the swelling analysis results for the different thicknesses of Membrane A in pure water. The mass of Membrane B increased on average $104 \pm 35\%$ after 3 days of immersion in pure water, which was considerably higher than that measured for Membrane A. The greater uptake of water by Membrane B may be attributed to the presence of water in its support layer (see Figure 1); however, the contribution of the polyester support could not be separated from that of the active layer. Water uptake by Membranes A and B plateaued following 24
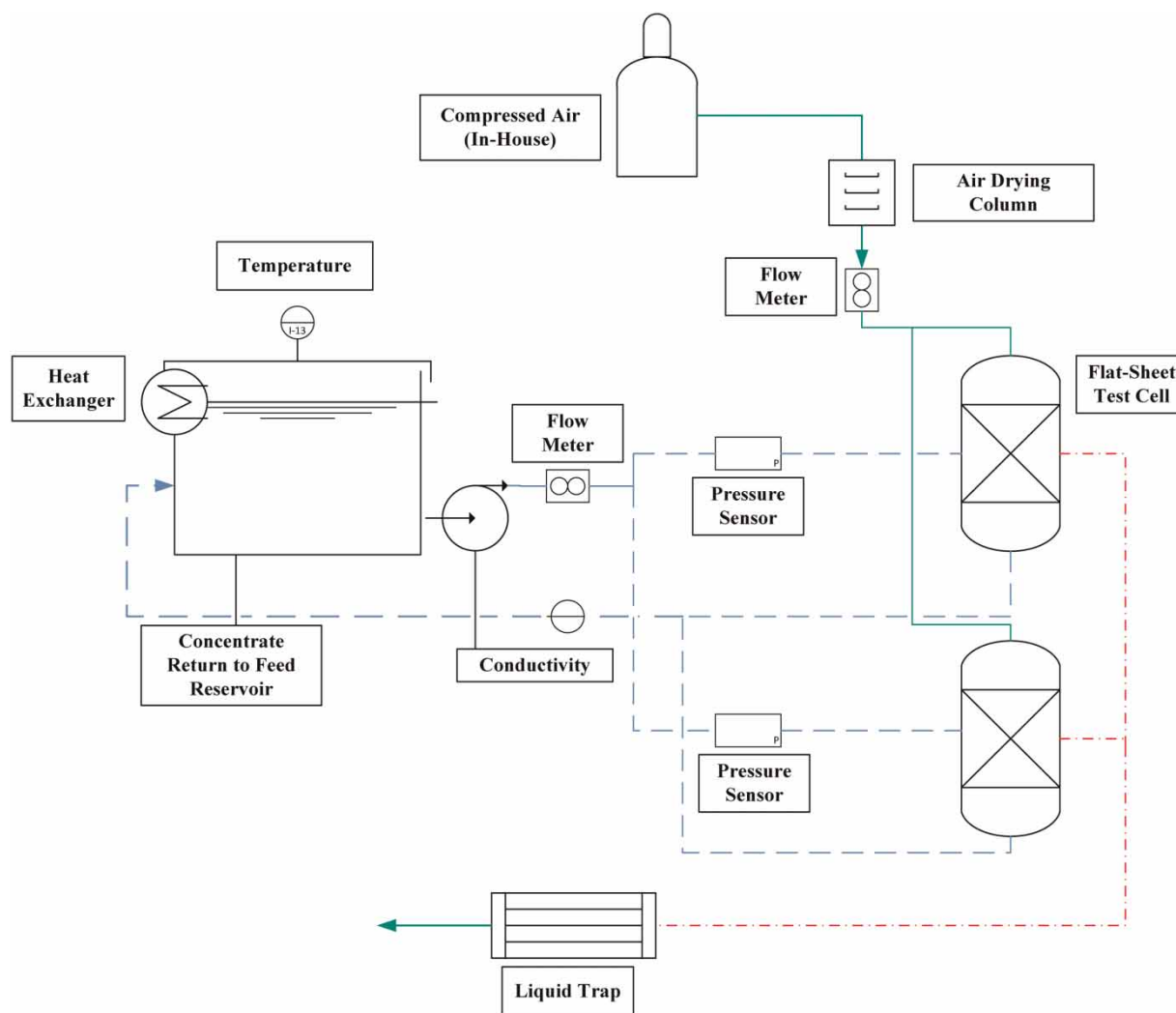
Figure 2 | Process flow diagram of the cross flow pervaporation test unit (dashed lines = liquid flow lines, solid lines = dry air flow lines, and dash-dot lines = moist air flow lines).

and 12 h, respectively. Both Membrane A ($\theta_{H2O} = 46.1 \pm 2.97°$) and Membrane B ($\theta_{H2O} = 11.8 \pm 4.70°$) were characterized as being hydrophilic polymers, with Membrane B having a higher affinity (lower θ_{H2O}) for water than Membrane A. Therefore, based on these two types of analyses, Membrane B had a higher affinity for water than did Membrane A.

Salts in solution can affect the diffusion coefficient of water molecules through a pervaporation membrane, and in turn affect the water flux through a variety of avenues such as osmotic de-swelling. It is known that the fractional free volume space in water swollen polymers is proportional to the polymer's water content (Hodge *et al.* 1996; Ju *et al.*

2010). So, as a polymer swells and absorbs water, the unoccupied space within the polymer matrix increases and so does the amount of free volume within the polymer. It has also been found that water sorption by polymers generally decreases as the thermodynamic activity of the surrounding water decreases (Jeck *et al.* 2009; Geise *et al.* 2013). As the salt concentration of a given water increases, the thermodynamic activity of the water decreases (Moggia & Bianco 2007). The reason for the decreased water uptake by polymers due to the decreased activity of the solution is not yet well understood, but one explanation is that the solvent uptake of a cross-linked polymer is determined by a balance between the internal osmotic pressure of the pore liquid and the elastic

Table 1 | Summary of known and calculated membrane and system parameters that were used to model the permeate flux for Membranes A and B

Variable	Unit	Value	Source
D_i	$cm^2 \, s^{-1}$	Membrane A: 2.18×10^{-5} Membrane B: 1.58×10^{-6}	Averaged from values for various types of rubbery polymeric membranes (Baker 2004) Literature value for the CTA (Han *et al.* 2013)
$\gamma_{io(m)}$	Unitless	1	Equal to 1 for pure water (Sawyer *et al.* 2002)
γ_{io}^G	Unitless	1	Equal to 1 when reactions take place near atmospheric conditions (Sawyer *et al.* 2002)
m_i	$g \, mol^{-1}$	18.02	Molecular weight of water
ρ_m	$mol \, cm^{-3}$	Membrane A: 3.97×10^{-5} Membrane B: 2.62×10^{-5}	Calculated from using reported values for density ($1.31 \, g \, cm^{-3}$) and molecular weight ($50{,}000 \, g \, mol^{-1}$) Calculated from the reported membrane density ($1.19 \, g \, cm^{-3}$) and average molecular weight for CTA ($30{,}000 \, g \, mol^{-1}$) (Han *et al.* 2013)
p_{io}	Pa	2350–12,332	Calculated for each experimental condition using: $p_{io} = 133.22 \times e^{(20.386-(5132/T))}$
p_{il}	Pa	55.5–60.8	Calculated based on the measured relative humidity (*RH*) of the gas phase: $RH, \% = 100 \times p_{il}/p_{isat}$
p_{isat}	Pa	2275–2309	Calculated at room temperature using: $p_{isat} = (e^{77.3507 \times T - (72.35/T)})/T^{8.2}$
l	cm	Membrane A: 0.002–0.025 Membrane B: 0.001	Measured value Measured thickness of the active layer (Membrane B)

forces of the polymer matrix that occur from the expansion of the polymer molecules during solvent absorption (Choi & Datta 2003). Osmotic de-swelling refers to decreased polymer swelling due to the presence of salts in the bulk solution (Khare & Peppas 1995). Osmotic de-swelling, therefore, corresponds to a reduction in the fractional free volume within the nonporous membrane. For both Membrane A and B the amount of water that was adsorbed by the membrane polymer varied slightly as a function of solution ionic strength (0–1 M NaCl); however, the results were not significantly different from one another based on a two tailed *t*-test ($n = 5$) of the respective data sets. Similarly, no statistical difference existed between the amount of water adsorbed by the membrane polymers when they were immersed in the saline solutions and DDW. Therefore, salts were not affecting in a significant way the interactions between water molecules and the two types of membrane polymers.

Relationships between water flux, water temperature, and membrane thickness

The specific flux of Membrane $A_{20 \, \mu m}$ was determined to be $5.95 \times 10^{-9} \, m^3 \, m^{-2} \, day^{-1} \, Pa^{-1}$. The average specific flux for Membrane B was determined to be $3.32 \times 10^{-7} \, m^3 \, m^{-2} \, day^{-1} \, Pa^{-1}$, which was two orders of magnitude greater than that measured for Membrane A. The hydraulic resistance

(R_m), where R_m is calculated using Darcy's Law ($R_m = [\Delta P - \Delta \pi]/[\mu \times J]$), established values for both membranes were on the order of $10^{-10} \, m^{-1}$. The magnitude of the R_m values for both membranes makes them comparable to a tight RO membrane ($R_m \geq 10^{10} \, m^{-1}$). Both membranes had specific flux values that were comparable to literature values for other nonporous pervaporation membranes (Korin *et al.* 1996; Yeom *et al.* 2001; Namboodiri & Vane 2007). Differences in specific fluxes are attributed to differences in membrane material chemistry, namely its affinity for water, and structure (fractional free-volume-space).

Permeate flux as a function of vapor pressure gradient (ΔVP) was also measured for the two types of membranes (Figure 3). For Membrane A, the permeate flux was measured for each of the different membrane thicknesses (Figure 3(a)). From Figure 3(a), the permeate flux increased with increasing ΔVP for each of the different membrane thicknesses; however, the increase was more substantial for the thinner membranes (thickness $\leq 50 \, \mu m$). From $\Delta VP = 2300 \, Pa$ to $\Delta VP = 12{,}275 \, Pa$, the permeate flux increased by approximately 150% for Membrane $A_{20 \, \mu m}$ and by approximately 41% for Membrane $A_{50 \, \mu m}$. Increases in fluxes for Membrane $A_{90 \, \mu m}$ and Membrane $A_{250 \, \mu m}$ were 7 and 13%, respectively, over the same ΔVP range.

Permeate fluxes for Membrane B were much higher than that measured for Membrane A regardless of the ΔVP and/or
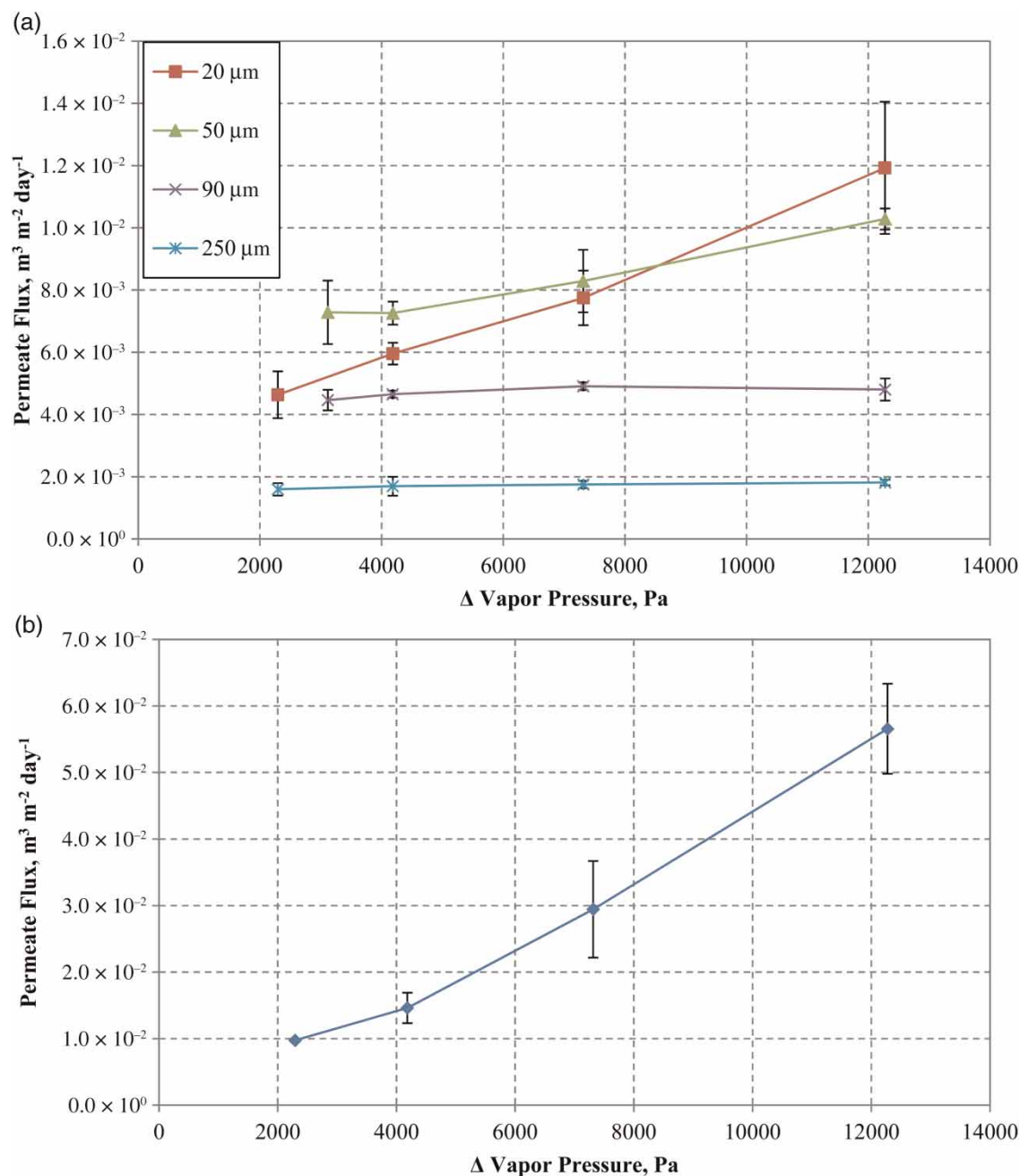
Figure 3 | Permeate flux as a function of the vapor pressure differential between the feed and the permeate phases for (a) Membrane A and (b) Membrane B. The feed water used was doubly deionized water (pH = 5.5). The error bars represent the standard deviation in the reported flux values based on three replicate measurements ($n = 3$).

membrane thickness studied. For the largest vapor pressure gradient analyzed ($\Delta VP = 12{,}275$ Pa), the measured flux for Membrane B was approximately five times that of the thinnest Membrane A (5.65×10^{-2} m^3 m^{-2} day^{-1} vs. 1.19×10^{-2} m^3 m^{-2} day^{-1}). The permeate fluxes for Membrane B increased 400% over the studied range of ΔVP (Figure 3(b)).

The average specific flux for Membrane A was determined using the sweeping gas configuration across all thickness values and was 1.04×10^{-6} m^3 m^{-2} day^{-1} Pa^{-1}. Specific flux decreased linearly ($R^2 = 0.88$) with an increase in membrane thickness. For example, the average specific flux for Membrane A$_{20\,\mu m}$ was 1.37×10^{-6} m^3 m^{-2} day^{-1} Pa^{-1},

while that for Membrane $A_{250\,\mu m}$ was $3.73 \times 10^{-7}\,m^3\,m^{-2}\,day^{-1}\,Pa^{-1}$. The average specific flux for Membrane B was $4.09 \times 10^{-6}\,m^3\,m^{-2}\,day^{-1}\,Pa^{-1}$, which was of the same magnitude as that measured for Membrane $A_{20\,\mu m}$.

The specific flux of each membrane was determined using the sweeping gas operation scheme and was roughly three orders of magnitude greater than that determined using the dead end filtration approach for Membrane A. A one order of magnitude difference also existed in the specific flux values for Membrane B. In both cases the measured specific flux was higher when determined using the sweeping gas approach. This difference may be attributed to compression of the membrane materials during testing with the dead end configuration; however, both membranes were compressed prior to carrying out the experiments. Another possibility is that the fundamental mechanisms that drive water transport through the membrane change when the driving force (hydraulic pressure vs. ΔVP) for the process changes.

A two-factor, completely randomized design (CRD) one way analysis of variance (ANOVA) was performed to determine which factors had a significant effect on the measured permeate flux. The two factors considered in this analysis were membrane thickness and ΔVP. Significance was determined for both factors (membrane thickness $p \leq 0.0001$ and ΔVP $p = 0.0004$). A least significant difference (LSD) post hoc analysis was performed on both the ΔVP and membrane thicknesses. All values of ΔVP were found to have a statistically significant difference in impact on the permeate fluxes. Statistically significant differences in fluxes were detected between Membrane A having thicknesses of 20, 50, 90, and $250\,\mu m$ as well as Membrane B, but no statistically significant difference was detected in the fluxes measured for Membrane $A_{20\,\mu m}$ and Membrane $A_{50\,\mu m}$. These results indicate that both membrane thickness and ΔVP significantly affect the permeate fluxes, confirming that these values contribute to the governing mechanisms of transport through the hydrophilic membranes.

Results from the sweeping gas experiments were used to elucidate the different variables that are used to calculate the flux in pervaporation applications (Equation (1))

$$J_i = \frac{D_i K_i^G (p_{io} - p_{il})}{l} \tag{1}$$

where J_i is the flux of component i ($g\,cm^{-2}\,s^{-1}$); K_i^G is the sorption coefficient of component i between the gas and membrane phases ($g\,cm^{-3}\,Pa^{-1}$); p_{io} is the partial vapor pressure of component i in contact with the membrane at the feed interface (Pa); p_{il} is the partial vapor pressure of component i in contact with the membrane at the permeate interface (Pa); and l is the thickness of membrane (cm). Values for the different variables used in the theoretical assessment of the flux values are summarized in Table 1.

The theoretical permeate fluxes for Membranes A and B, which were calculated using the associated variables given in Table 1, are plotted along with the measured flux values for both membranes in Figure 4. The measured data for each thickness of Membrane A were comparable to the theoretical curves (Figure 4(a)–(d)), whereas the measured data for Membrane B were as much as one order of magnitude greater than the theoretical data. The slope for the measured data for Membrane A, irrespective of thickness, was lower than that for the theoretical data. The opposite scenario occurred for Membrane B, where the measured results had a more substantial slope (Figure 4(e)).

Differences in the theoretical and measured data may be attributed to any number of incorrect assumptions that were made when using Equation (1) (Table 1). The variable that had the highest level of uncertainty was the diffusion coefficient of water (D_i) across each of the two membrane types. Therefore, this variable was used as a fitting parameter for the theoretical and measured data sets. In general, the value of D_i depends on both the properties of the permeating substance and the environment through which the substance is permeating. The D_i value assumed for Membrane A ($D_i = 2.18 \times 10^{-5}\,cm^2\,s^{-1}$) and Membrane B ($D_i = 1.58 \times 10^{-5}\,cm^2\,s^{-1}$) were based on values found in the literature (Brun *et al.* 1985; Sano *et al.* 1997; Jullok *et al.* 2012) and, therefore, are not specific to the membranes studied here. The best fit overall using D_i value (all membrane thicknesses and vapor pressure gradients) for Membrane A was $2.54 \times 10^{-5}\,cm^2\,s^{-1}$, while that for Membrane B was $2.27 \times 10^{-5}\,cm^2\,s^{-1}$. Using the fitted D_i values improved the agreement between the theoretical and measured fluxes as a function of ΔVP, with the exception of those results for Membrane $A_{20\,\mu m}$ (Figure 4(a)). This may be attributed to Membrane $A_{20\,\mu m}$ having a D_i that was unique from the other membrane thicknesses.
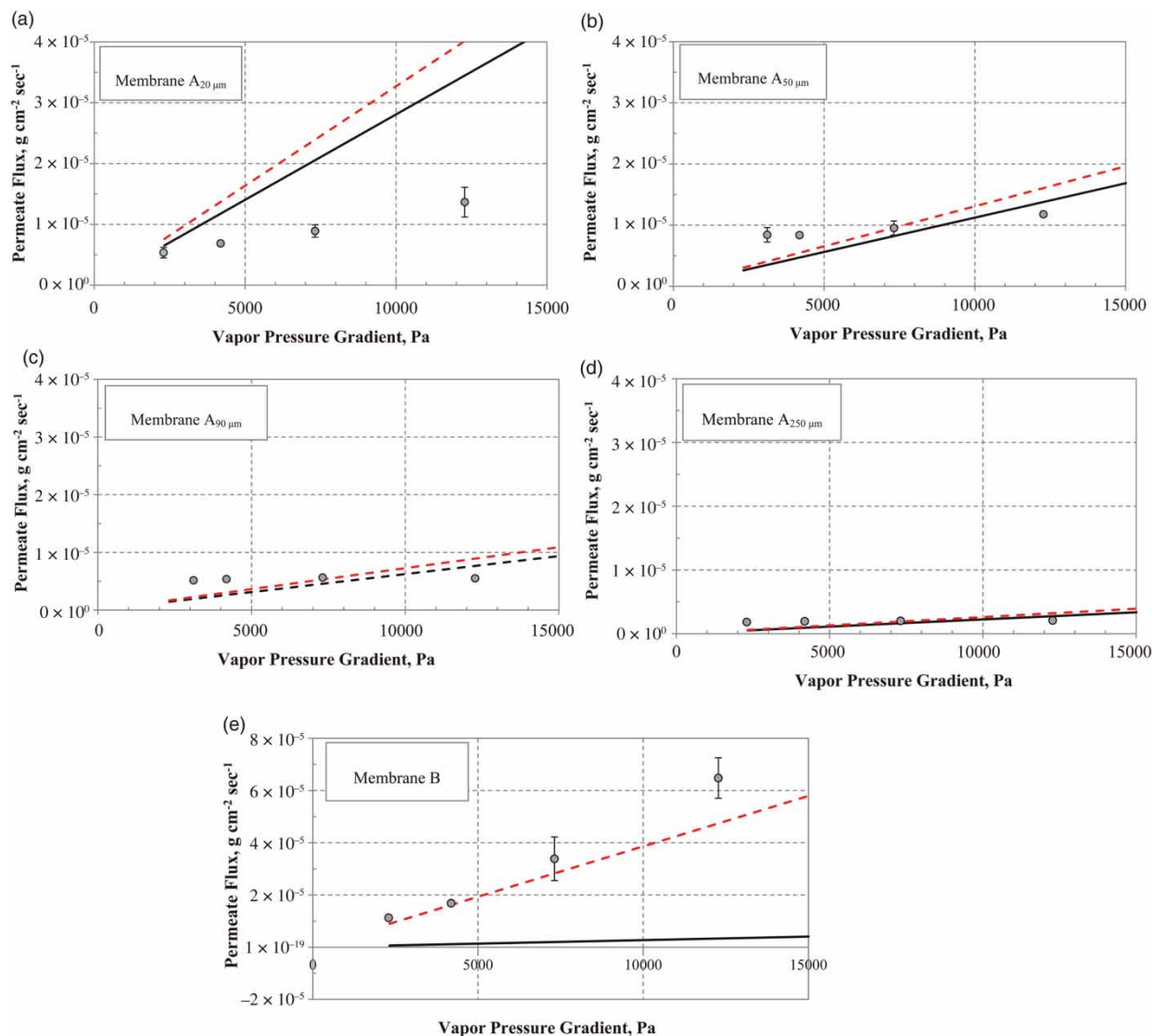
Figure 4 | Measured and theoretical flux values as a function of vapor pressure gradient for (a) Membrane $A_{20\,\mu m}$, (b) Membrane $A_{50\,\mu m}$, (c) Membrane $A_{90\,\mu m}$, (d) Membrane $A_{250\,\mu m}$, and (e) Membrane B. Measured flux values are represented by the solid circles (I = 0 mM, pH = 5.5, $n \geq 3$). The black/solid lines were calculated using literature values for the diffusion coefficient of water across the respective membranes (D_i). The red/dashed lines were calculated using D_i as a fitting parameter.

Another variable to consider is the impact that water temperature has on D_i. Changes in temperature can impact the polymeric structure of the membrane itself. As the temperature of the feed solution increases so does the thermal motion of the segments of the polymer backbone, which could lead to increased permeate diffusion coefficients, particularly for Membrane $A_{20\,\mu m}$. So the D_i values could potentially increase with an increase in temperature which could result in greater observed fluxes. This increase in D_i due to increased temperature was not taken into

account when calculating the theoretical fluxes. In fact, a two factor (vapor pressure gradient and membrane thickness) CRD one way ANOVA was performed on the fitted D_i values for Membrane A, and it was determined that both vapor pressure gradient and membrane thickness displayed statistical significance ($p \leq 0.0001$ for both ΔVP and l). An LSD post hoc test was performed on both factors. Membrane $A_{20\,\mu m}$ was determined to have a statistically significant different (smaller in value) D_i value than the other membrane thicknesses. A statistically significant difference

was detected in the D_i values for the highest ΔVP examined compared to the other ΔVP values. This shows that the Di value can vary not only for membranes of similar composition but also for the operating conditions at which it is used.

The theoretical and observed permeate fluxes were also plotted in terms of the membrane thickness (Figure 5). The theoretical flux was calculated using the averaged fitted D_i value for Membrane A. Note that Membrane B was not analyzed as it was only available in a singular thickness. For all ΔVP values, the theoretical water flux increased in a logarithmic fashion with decreasing membrane thickness. Above a threshold membrane thickness of approximately 100 μm, the water flux reached a plateau where large increases in membrane thickness resulted in small decreases in the theoretical water flux. Below a membrane thickness of 50 μm, the theoretical water flux increased nearly exponentially with decreasing membrane thickness. Therefore, the optimum thickness of the active layer for the pervaporation membranes would need to be ≤50 μm in order to maximize production efficiency.

There was general agreement between the model and observed data in that water flux generally decreased as the membrane thickness increased. Deviations between the measured and theoretical results did exist (see Figure 5) for the membrane having the highest fluxes (Membrane $A_{20\,μm}$). One possible explanation for this deviation could be some sort of internal concentration polarization effect taking place within the membrane material matrix. Because the driving force for mass transport in pervaporation is the

ΔVP, concentration polarization in this case refers to a build-up of water molecules within the membrane interior. In a nonporous hydrophilic membrane, water molecules must move down gradient through the polymer chain via the fractional free volume space (microcavities not occupied by the polymer chain). As more water molecules penetrate into the membrane (i.e. at higher fluxes), the moisture content within the membrane increases, creating a higher vapor pressure within the membrane material, thereby reducing the ΔVP. With the exception of Membrane $A_{20\,μm}$, the observed fluxes were consistently greater than the theoretical curves. If correct, internal concentration polarization as described here may be a limiting factor for fluxes in pervaporation applications.

Pervaporation membrane performance (flux and rejection) as a function of solute due to presence of solutes

Solutes impact membrane performance in a variety of manners including membrane fouling (e.g. mineral scaling if scale forming elements are present) (Shirazi *et al.* 2010) and concentration polarization (Sablani *et al.* 2001; Nagy 2010). While the relationships between fouling and the presence of solutes in feed waters are relatively well established for pressure-driven membrane processes (Howe & Clark 2002; Kim *et al.* 2009; Lin *et al.* 2010; Shirazi *et al.* 2010), they are less understood for non-pressure driven processes like membrane distillation (He *et al.* 2008; Goh *et al.* 2013) and pervaporation. This lack of understanding concerning the non-pressure driven process of pervaporation led to this evaluation of the effects of the presence of solutes (i.e. salts) in the feed water on permeate fluxes through the two types of pervaporation membranes.

Permeate flux was measured as a function of the NaCl concentration in the feed water for Membrane A and B, while maintaining a constant ΔVP of 12,275 Pa. From Figure 6(a), the permeate flux decreased as the salinity of the feed water increased. This impact was most pronounced for Membrane $A_{20\,μm}$, where the flux decreased by 90%. In comparison, the flux decreased by approximately 50% for the Membrane $A_{250\,μm}$. The relationship between the measured flux and solution ionic strength was not linear for Membrane A. The permeate flux for Membrane B also
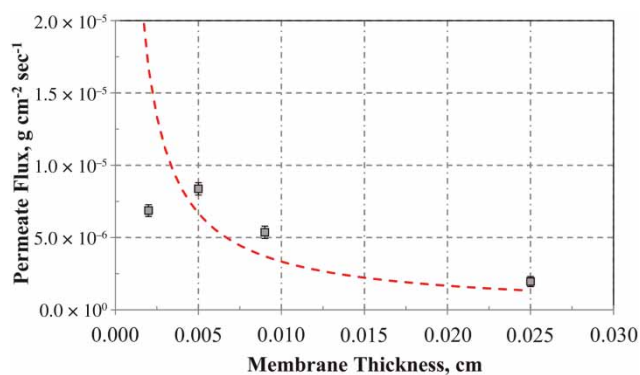

Figure 5 │ Measured and calculated permeate fluxes as a function of membrane thickness (I = 0 mM, pH = 5.5, ΔVP = 4185 Pa, $n \geq 3$).
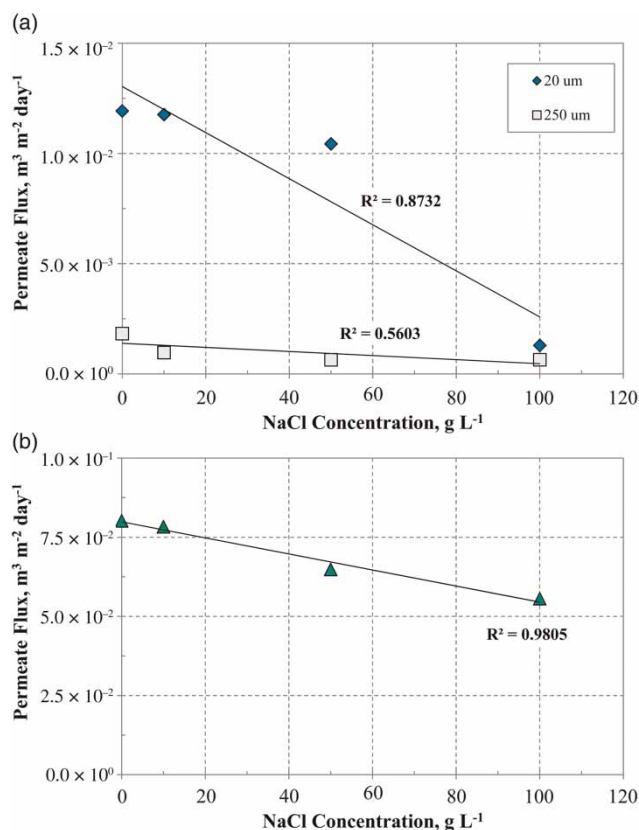
(a)

(b)

Figure 6 │ Permeate flux as a function of sodium chloride concentration for (a) Membrane $A_{20\,\mu m}$ and Membrane $A_{250\,\mu m}$ membranes and (b) Membrane B ($T = 50\,^{\circ}$C, RH sweeping gas = 2%, ΔVP = 12,275 Pa, pH = 5.5, $n \geq 3$).

decreased, but in a linear fashion, with increasing ionic strength (Figure 6(b)). The average flux decreased from 0.080 when treating pure water to 0.056 $\text{m}^3\,\text{m}^{-2}\,\text{day}^{-1}$ when treating a source water containing 100 g L^{-1} NaCl, which is a flux loss of 30%.

The decline in permeate flux with increasing salt concentrations as observed for Membranes A and B may be attributed to a variety of factors. First, the increase in NaCl concentration could lead to a decrease in the ΔVP, as the salt concentration affects (decreases) the vapor pressure of the feed solution (Fabuss & Korosi 1966). The vapor pressure of pure water at 50 °C is approximately 12.35 kPa, whereas the vapor pressure of water at 50 °C containing 100 g L^{-1} NaCl is 11.58 kPa, which is a difference of approximately 6%. Accounting for the theoretical drop in vapor pressure of the feed water as the salt concentration increased to 100 g L^{-1} NaCl, while keeping all other variables constant (Table 1), resulted in a 1–2% decrease in

the theoretical flux compared to that for pure water. This difference is less substantial than the observed flux loss that occurred for Membrane $A_{20\,\mu m}$ (90%) and Membrane B (30%). This indicates that while the decrease in vapor pressure due to an increase in salt concentration may slightly decrease the permeate fluxes for the pervaporation membranes, it does not account for all of the observed flux loss. Also of note is the fact that the amount of flux loss that was observed with increasing salt concentration varied depending on membrane type, thickness and observed water fluxes.

Other possible factors that may have impacted the water flux as the salt concentration increased include membrane fouling in the form of mineral scaling, concentration polarization effects from salt accumulation at the membrane surface, and changes in the affinity of water molecules with the membrane polymers. This latter factor may result from the decreased thermodynamic activity of the water from the increased salt (NaCl) concentration in the bulk solution and/or at the membrane-bulk solution interface (concentration polarization) (Sablani *et al.* 2001; Nagy 2010). The phenomenon of osmotic deswelling within the membrane could also be occurring. The increased salt concentration in the feed water results in decreased thermodynamic activity of the water, which may lead to decreased solvent (water) uptake by the membrane; however, no significant difference was observed in the amount of water that was adsorbed by either membrane type across the salt concentrations studied here. Therefore, while osmotic deswelling may be playing some role it is not likely the sole contributor to the decrease in flux with increasing salt concentration.

In general, spacers can help create turbulence at the interface between the membrane surface and the feed solution, which subsequently increases the magnitude of the shear forces acting on particles or dissolved substances that accumulate at the membrane surface (Shrivastava *et al.* 2008; Mo & Ng 2010; Saeed *et al.* 2012). In this way, spacers may be used to mitigate the formation of polarization layers at membrane–solution interfaces. Increased mixing at the membrane surface also reduces the effects associated with temperature polarization across the membrane. Temperature polarization occurs as heat is transferred across the membrane from the feed to the permeate phases (Cath *et al.* 2004). Heat transfer results in the

temperature at the membrane-feed solution interface, as well as the interface between the membrane and permeate phase, being respectively lower and higher than the bulk values. This in turn reduces ΔVP, which is the driving force for mass transport in pervaporation.

Because the test solutions used here were comprised of sodium chloride, membrane fouling through scale formation was not likely to occur. Concentration polarization at the membrane–feed solution interface was likely; however, increases in the local salt concentration were previously shown to have minimal effects on the vapor pressure of the feed solution. Therefore, changes in the vapor pressure of the feed solution was discounted as a significant contributor to flux decline. Flux was observed to decrease with increasing salt concentration in the feed solution (Figure 6). So an increase in the salt concentration at the membrane-solution interface would in turn result in a decline in the measured flux, though the reason for this remains unclear. Our working assumption was that if concentration and temperature polarization was in fact degrading the performance of the different membranes, then inclusion of the feed spacers would improve their performance.

Permeate flux data for Membrane $A_{20\ \mu m}$ with and without feed spacers are given in Figure 7. The permeate flux for Membrane $A_{20\ \mu m}$ increased 590% when feed spacers were included while holding the sweeping gas velocity constant. The flux increased by a full order of magnitude when the sweeping gas velocity was increased from 0.075 to 0.170 m s^{-1}. The increase in fluxes for Membrane $A_{20\ \mu m}$ due to the addition of the feed spacer was likely due to a

reduction in the thicknesses of the concentration and temperature polarization layers at the membrane surface; however, the exact mechanism by which this affected the water flux is unclear. Increasing the sweeping gas velocity increases the efficiency by which moisture is removed from the permeate side of the membrane. In turn, this maintains a greater ΔVP across the membrane and hence a higher flux. Therefore, the integration of spacers and optimization of sweeping gas conditions are two strategies which can be used to maximize the performance of pervaporation processes.

Both Membranes A and B were found to reject salts very well, (rejection $\geq 99\%$) irrespective of the feed solution ionic strength. FESEM-EDS images of the permeate sides of Membranes A and B (data not shown) showed an absence of any salt cake, indicating that the salts were being retained by the membranes. The absence of any salts on the permeate sides of the membranes demonstrated that the measured rejection values were due to separation by the membrane and not simple evaporation of the permeate from the membrane surface. Rejection was thus attributed, at least in part, to conventional rejection mechanisms by nonporous membranes as covered in the solution diffusion model of separation. It was clear from the rejection data that the pervaporation membranes were rejecting salts; however, the rejection was <100%, indicating that some fraction of salts were penetrating into and passing through the membrane material over time.

An elemental analysis of the membranes after operation was completed by determining a relative concentration of a given element (from the EDS spectra data), which was compared to the relative concentration of that element in the same general location of a virgin membrane sample. The percent increase in the relative concentration of a given element was then calculated. The intent of this analysis is to determine if electrostatic and/or steric interactions are playing any role in the separation of ions by the different pervaporation membranes.

Images and elemental analysis of membrane samples used in the sweeping gas experiments are shown in Figures 8 and 9. Salt crystals can be seen on the feed surface of Membrane $A_{20\ \mu m}$ (Figure 8), and areas of relatively high atomic mass (displayed as bright/white spots). No crystals or salt deposits were observed on the permeate side of the membrane. The concentrations of sodium and chloride were found to increase
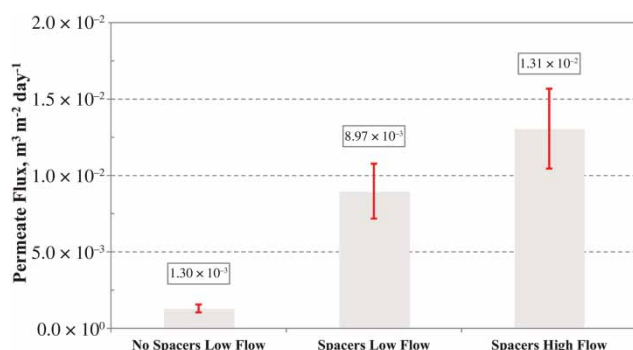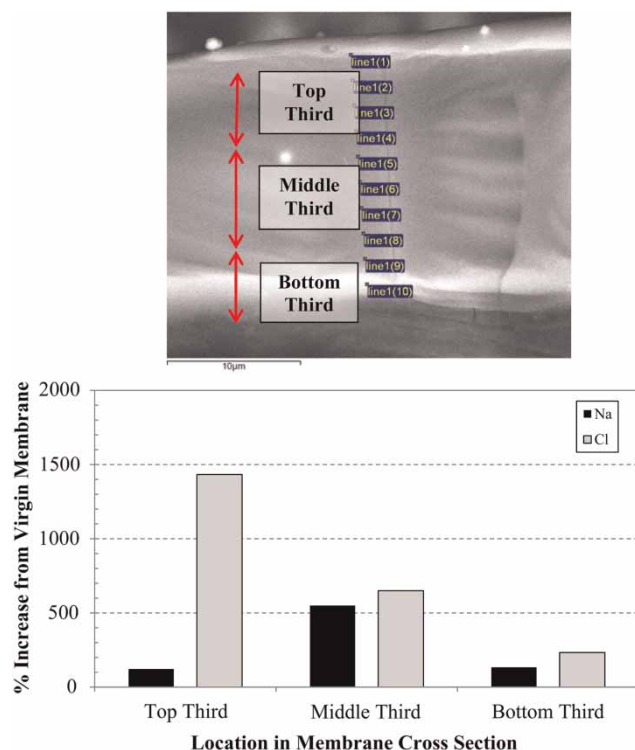
Figure 7 | Permeate flux values for Membrane $A_{20\ \mu m}$ as a function of sweeping gas velocity and the absence/presence of feed spacers (low flow = 0.075 m s^{-1}, high flow = 0.170 m s^{-1}, [NaCl] = 100 g L^{-1} NaCl, pH = 5.5, T = 50 °C, RH sweeping gas = 2%, ΔVP = 12,275 Pa, $n \geq 3$).

122   E. Huth et al.   Pervaporation desalination of highly saline source waters

Journal of Water Reuse and Desalination | 04.2 | 2014

Figure 8 | (Top) Representative back scattered electron detector (BSED) FESEM image of Membrane $A_{20\,\mu m}$ after treating a solution of sodium chloride ([NaCl] = 100 g L^{-1}, pH = 5.5, T = 50 °C, RH sweeping gas = 2%, ΔVP = 12,275 Pa). (Bottom) Relative increase in the concentrations of sodium (Na) and chloride (Cl) throughout the depth of Membrane $A_{20\,\mu m}$ relative to the measured concentration in the virgin membrane sample.
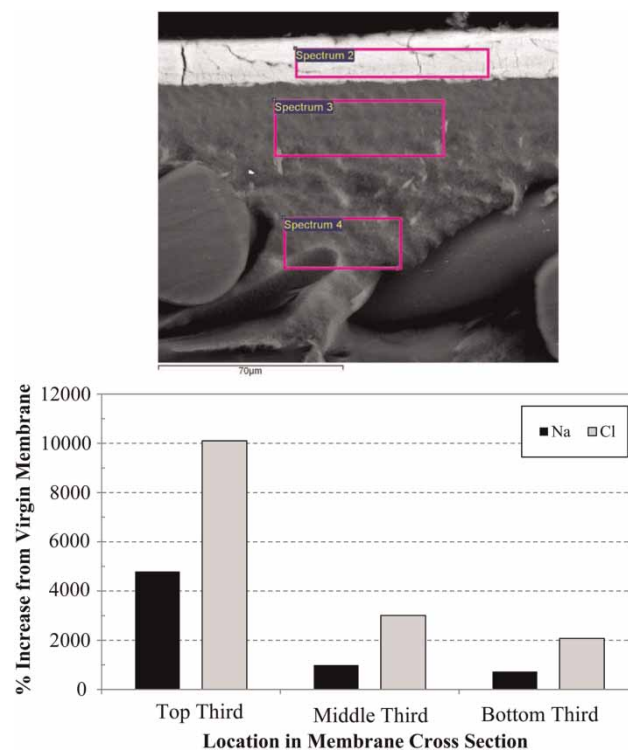

Figure 9 | (Top) Representative BSED FESEM image of Membrane B after treating a solution of sodium chloride ([NaCl] = 100 g L^{-1}, pH = 5.5, T = 50 °C, RH sweeping gas = 2%, ΔVP = 12,275 Pa). (Bottom) Relative increase in the concentrations of sodium (Na) and chloride (Cl) throughout the depth of Membrane B relative to the measured concentration in the virgin membrane sample.

throughout the entire thickness of Membrane $A_{20\,\mu m}$ (Figure 8) relative to that measured for the virgin membrane sample. A similar observation was made for Membrane B (Figure 9). However, the chloride concentration did appear to increase to a greater extent near the feed side of both membranes. Because the EDS measurement does not provide an actual concentration value, we can only determine if the amount of an element is more prevalent in the sample. The substantial increase, reported in terms of a percent increase, in sodium and chloride concentrations in the two types of membranes is due to the fact that neither virgin material contained measurable amounts of these elements. So the increase in the relative amount of a given element should not be viewed in terms of large amounts of salts entering the membrane. Keeping in mind that Membrane $A_{20\,\mu m}$ and Membrane B were characterized by a net negative charge under these test conditions, the ability of a given ion to penetrate into the membrane material matrix would appear to be governed at

least in part by electrostatic interactions. Therefore, co-ions would pass through the membranes more readily than counter ions. In this case, the anion appeared to enter both membranes more readily than did the cation. Note that steric interactions may also play a role as the chloride has a smaller radius of hydration relative to the sodium cation.

CONCLUSIONS

Permeate flux is a significant function of two membrane properties, which are: (1) the thickness of the active separating layer; and (2) the diffusion coefficient (D_i) of water through the membrane. Membrane B demonstrated superior flux properties relative to Membrane A because of its more hydrophilic character and thinner separating layer. Permeate flux was affected by changes in feed solution ionic strength, which was a complex function of the membrane properties and process operating conditions. Further

optimization of Membrane B for pervaporation applications must focus on reducing the thickness of the active layer and improving its salt rejection properties. Inclusion of spacers on the feed side of the membrane increased mixing conditions at the membrane-bulk solution interface, resulting in improved fluxes for both Membrane A and B. These results demonstrate the feasibility of pervaporation processes for desalination of high-salinity brines and thus providing a new technique for managing produced waters.

ACKNOWLEDGEMENTS

REFERENCES

Adham, S., Hussain, A., Matar, J. M., Dores, R. & Janson, A. 2013 Application of membrane distillation for desalting brines from thermal desalination plants. *Desalination* **314**, 101–108.

Alkhudhiri, A., Darwish, N. & Hilal, N. 2013 Produced water treatment: application of air gap membrane distillation. *Desalination* **309**, 46–51.

Baker, R. 2004 *Membrane Technology and Applications*. 2nd edn, John Wiley & Sons Ltd, Chichester, UK.

Beckman, A., Ambulkar, A., Umble, A., Rosso, D., Husband, J., Cleary, J., Sandino, J., Goldblatt, M., Horres, R., Neufeld, R., Mau, R. & Jeyanayagam, S. 2013 Considerations for accepting fracking wastewater at water resource recovery facilities. *Water Environ. Fed.* 4 pp.

Benko, K. L. & Drewes, J. E. 2008 Produced water in the western United States: geographical distribution, occurrence, and composition. *Environ. Eng. Sci.* **25** (2), 239–246.

Brant, J. A. & Childress, A. E. 2002 Assessing short-range membrane-colloid interactions using surface energetics. *J. Membr. Sci.* **203**, 257–273.

Brun, J. P., Larchet, C., Melet, R. & Bulvestre, G. 1985 Modelling of the pervaporation of binary mixtures through moderately swelling, non-reacting membranes. *J. Membr. Sci.* **23**, 257–283.

Cath, T. Y., Adams, V. D. & Childress, A. E. 2004 Experimental study of desalination using direct contact membrane distillation: a new approach to flux enhancement. *J. Membr. Sci.* **228** (1), 5–16.

Choi, P. & Datta, R. 2003 Sorption in proton-exchange membranes an explanation of Schroeder's paradox. *J. Electrochem. Soc.* **150** (2), E601–E607.

Clark, C. E. & Veil, J. A. 2009 *Produced Water Volumes and Management Practices in the United States*. Argonne National Laboratory, IL, USA, 60 pp.

Drobek, M., Yacou, C., Motuzas, J., Julbe, A., Ding, L. P. & da Costa, J. C. D. 2012 Long term pervaporation desalination of tubular MFI zeolite membranes. *J. Membr. Sci.* **415**, 816–823.

Fabuss, B. M. & Korosi, A. 1966 Vapor pressures of binary aqueous solutions of NaCl, KCl, Na2SO4 and MgSO4 at concentrations and temperatures of interest in desalination processes. *Desalination* **1**, 139–148.

Geise, G. M., Freeman, B. D. & Paul, D. R. 2013 Sodium chloride diffusion in sulfonated polymers for membrane applications. *J. Membr. Sci.* **427**, 186–196.

Goh, S., Zhang, Q., Zhang, J., McDougald, D., Krantz, W. B., Liu, Y. & Fane, A. G. 2013 Impact of a biofouling layer on the vapor pressure driving force and performance of a membrane distillation process. *J. Membr. Sci.* **438**, 140–152.

Han, J., Cho, Y. H., Kong, H., Han, S. & Park, H. B. 2013 Preparation and characterization of novel acetylated cellulose ether (ACE) membranes for desalination applications. *J. Membr. Sci.* **428**, 533–545.

He, F., Gilron, J., Lee, H., Song, L. & Sirkar, K. K. 2008 Potential for scaling by sparingly soluble salts in crossflow DCMD. *J. Membr. Sci.* **311** (1–2), 68–80.

Hickenbottom, K. L., Hancock, N. T., Hutchings, N. R., Appleton, E. W., Beaudry, E. G., Xu, P. & Cath, T. Y. 2013 Forward osmosis treatment of drilling mud and fracturing wastewater from oil and gas operations. *Desalination* **312**, 60–66.

Hodge, R. M., Bastow, T. J., Edward, G. H., Simon, G. P. & Hill, A. J. 1996 Free volume and the mechanism of plasticization in water-swollen poly(vinyl alcohol). *Macromolecules* **29** (25), 8137–8143.

Howe, K. J. & Clark, M. M. 2002 Fouling of microfiltration and ultrafiltration membranes by natural waters. *Environ. Sci. Technol.* **36**, 3571–3576.

IEA Press Release 2012 International Energy Agency, North America leads shift in global energy balance, IEA says in latest World Energy Outlook. Available from: www.iea.org/newsroomandevents/pressreleases/2012/november/name,33015,en.html.

Jeck, S., Scharfer, P. & Kind, M. 2009 Water sorption in physically crosslinked poly(vinyl alcohol) membranes: An experimental investigation of Schroeder's paradox. *J. Membr. Sci.* **337**, 291–296.

Ju, H., Sagle, A. C., Freeman, B. D., Mardel, J. I. & Hill, A. J. 2010 Characterization of sodium chloride and water transport in crosslinked poly(ethylene oxide) hydrogels. *J. Membr. Sci.* **358**, 131–141.

Jullok, N., Deforche, T., Luis, P. & Van der Bruggen, B. 2012 Sorption and diffusivity study of acetic acid and water in polymeric membranes. *Chem. Eng. Sci.* **78**, 14–20.

Kharak, Y. K., Thordsen, J. J., Conaway, C. H. & Thomas, R. B. 2013 The energy-water nexus: potential groundwater-quality degradation associated with production of shale gas. *Procedia Earth Planet. Sci.* **7**, 417–422.

Khare, A. R. & Peppas, N. A. 1995 Swelling/deswelling of anionic copolymer gels. *Biomaterials* **16**, 559–567.

Kim, S., Kim, C.-H., Lee, E., Lee, S., Sarper, S. & Cho, J. 2009 Enhanced or reduced concentration polarization by membrane fouling in seawater reverse osmosis (SWRO) processes. *Desalination* **247**, 162–168.

Korin, E., Ladizhensky, I. & Korngold, E. 1996 Hydrophilic hollow fibre membranes for water desalination by the pervaporation method. *Chem. Eng. Process.* **35**, 451–457.

Korngold, E., Korin, E. & Ladizhensky, I. 1996 Water desalination by pervaporation with hollow fibre membranes. *Desalination* **107**, 121–129.

Lee, S., Boo, C., Elimelech, M. & Hong, S. 2010 Comparison of fouling behavior in forward osmosis (FO) and reverse osmosis (RO). *J. Membr. Sci.* **365**, 34–39.

Lin, J. C. T., Lee, D. J. & Huang, C. P. 2010 Membrane fouling mitigation: membrane cleaning. *Separ. Sci. Technol.* **45**, 858–872.

Lipski, C. & Cote, P. 1990 The use of pervaporation for the removal of organic contaminants from water. *Environ. Prog.* **9** (4), 254–261.

McCutcheon, J. R. & Elimelech, M. 2006 Influence of concentrative and dilutive internal concentration polarization on flux behavior in forward osmosis. *J. Membr. Sci.* **284** (1–2), 237–247.

McGinnis, R. L., Hancock, N. T., Nowosielski-Slepowron, M. S. & McGurgan, G. D. 2013 Pilot demonstration of the NH3/CO2 forward osmosis desalination process on high salinity brines. *Desalination* **312**, 67–74.

McKenzie, L. M., Witter, R. Z., Newman, L. S. & Adgate, J. L. 2012 Human health risk assessment of air emissions from development of unconventional natural gas resources. *Sci. Total Environ.* **424**, 79–87.

Michaels, A. S., Bixler, H. J. & Hodges Jr., R. M. 1965 Kinetics of water and salt transport in cellulose acetate reverse osmosis desalination membranes. *J. Colloid Sci.* **20** (9), 1034–1056.

Mo, H. & Ng, H. Y. 2010 An experimental study on the effect of spacer on concentration polarization in a long channel reverse osmosis membrane cell. *Water Sci. Technol.* **61**, 2035–2041.

Moggia, E. & Bianco, B. 2007 Mean activity coefficient of electrolyte solutions. *J. Phys. Chem. B* **111**, 3183–3191.

Mondal, S., Hsiao, C. L. & Ranil Wickramasinghe, S. 2008 Nanofiltration/reverse osmosis for treatment of coproduced waters. *Environ. Prog.* **27**, 173–179.

Nagy, E. 2010 Coupled effect of the membrane properties and concentration polarization in pervaporation: Unified mass transport model. *Separ. Purif. Technol.* **73**, 194–201.

Namboodiri, V. V. & Vane, L. M. 2007 High permeability membranes for the dehydration of low water content ethanol by pervaporation. *J. Membr. Sci.* **306**, 209–215.

Quinones-Bolanos, E., Zhou, H. D. & Parkin, G. 2005a Membrane pervaporation for wastewater reuse in microirrigation. *J. Environ. Eng. ASCE* **131** (12), 1633–1643.

Quinones-Bolanos, E., Zhou, H. D., Soundararajan, R. & Otten, L. 2005b Water and solute transport in pervaporation hydrophilic membranes to reclaim contaminated water for micro-irrigation. *J. Membr. Sci.* **252** (1–2), 19–28.

Sablani, S. S., Goosen, M. F. A., Al-Belushi, R. & Wilf, M. 2001 Concentration polarization in ultrafiltration and reverse osmosis: a critical review. *Desalination* **141**, 269–289.

Saeed, A., Vuthaluru, R., Yang, Y. W. & Vuthaluru, H. B. 2012 Effect of feed spacer arrangement on flow dynamics through spacer filled membranes. *Desalination* **285**, 163–169.

Sano, T., Ejiri, S., Yamada, K., Kawakami, Y. & Yanagishita, H. 1997 Separation of acetic acid-water mixtures by pervaporation through silicalite membrane. *J. Membr. Sci.* **123**, 225–233.

Sawyer, C., McCarty, P. & Parkin, G. 2002 *Chemistry for Environmental Engineering and Science*. McGraw Hill, New York.

Shao, P. & Huang, R. Y. M. 2007 Polymeric membrane pervaporation. *J. Membr. Sci.* **287** (2), 162–179.

Shirazi, S., Lin, C.-J. & Chen, D. 2010 Inorganic fouling of pressure-driven membrane processes – A critical review. *Desalination* **250**, 236–248.

Shrivastava, A., Kumar, S. & Cussler, E. L. 2008 Predicting the effect of membrane spacers on mass transfer. *J. Membr. Sci.* **323**, 247–256.

Singh, D. & Sirkar, K. K. 2012 Desalination of brine and produced water by direct contact membrane distillation at high temperatures and pressures. *J. Membr. Sci.* **389**, 380–388.

Slater, C. S., Schurmann, T., MacMillian, J. & Zimarowski, A. 2006 Separation of diactone alcohol-water mixtures by membrane pervaporation. *Separ. Sci. Technol.* **41**, 2733–2753.

Voros, N. G., Maroulis, Z. B. & Marinos-Kouris, D. 1996 Salt and water permeability in reverse osmosis membranes. *Desalination* **104**, 141–154.

Yang, M., Ju, Y. W., Tong, L. & Xu, G. 2011 Characteristics of coalbed produced water in the process of coalbed methane development. *Environ. Eng. Manage. J.* **10** (7), 985–993.

Yeom, C. K., Lee, S. H. & Lee, J. M. 2001 Pervaporative permeations of homologous series of alcohol mixtures through a hydrophilic membrane. *J. Appl. Polym. Sci.* **79** (4), 703–713.

Zhang, X., Cahill, D. G., Coronell, O. & Mariñas, B. J. 2007 Partitioning of salt ions in FT30 reverse osmosis membranes. *Appl. Phys. Lett.* **91**, 181904–181907.

Zwijnenberg, H. J., Koops, G. H. & Wessling, A. 2005 Solar driven membrane pervaporation for desalination processes. *J. Membr. Sci.* **250** (1–2), 235–246.